JMEPEG (2007) 16:155–162
DOI: 10.1007/s11665-007-9026-2

1059-9495/$19.00

Experimental and Numerical Simulation of Tensile Behavior and Failure of Titanium Alloys Under Simulated SPF Post-Processing Conditions

Franna Pitt, S. Abhyankar, P. Labossiere, and M. Ramulu

(Submitted April 20, 2006; in revised form October 22, 2006)

Three titanium alloys were tested in tension after simulated SPF exposure to three different temperatures and subject to three different post-processing methods. This paper presents an experimental analysis and numerical simulation of the mechanical behavior of post processed and as exposed titanium material. Stress versus strain curves, necking behavior and final fracture results were simulated using finite element modeling techniques and correlated to the experimental results. The simulations were able to predict experimental results in most cases.

Keywords numerical simulation, superplastic forming, tensile, titanium alloys

1. Introduction

Superplastic forming (SPF) is utilized to an increasing degree in fabricating metal parts in multiple industries, including aerospace. Superplastically formed parts offer weight and especially cost savings when compared to traditional methods of fabricating built up structure using fasteners and/or welding. Little has changed in the three decades of using SPF, yet improvements must be made to increase efficiency, conserve valuable resources and compete effectively in today's manufacturing environment. Lowering the SPF temperature is one possible improvement that would result in significant multiple benefits (Ref 1). Any change in processing, however, must be backed up by data showing that form, fit and function of the affected parts is not compromised.

Tensile properties are of primary importance in characterizing the mechanical behavior of materials. The standard tensile test yields considerable information about static material properties (Ref 2). These properties are essential in developing numerical models for predicting material behavior.

This article was presented at the AeroMat Conference, International Symposium on Superplasticity and Superplastic Forming (SPF) held in Seattle, WA, June 6-9, 2005.

Franna Pitt, S. Abhyankar, P. Labossiere, and **M. Ramulu,** Department of Mechanical Engineering, University of Washington, Box 352600, Seattle, WA 98195; and **Franna Pitt,** The Boeing Company, Box 3707, Seattle, WA 98124. Contact e-mail: franna.s.pitt@boeing.com.

In recent years, several finite element analysis formulations have been developed for plasticity framework. These formulations have been validated for cylindrical specimens loaded in tension. None, however, has focused on tensile loading of sheet material which has been exposed to SPF conditions. The purpose of this paper is to present an experimental analysis and numerical simulation of mechanical behavior during uniaxial tensile loading of titanium sheet material. The experimental procedure is described in Sec. 2 and in more detail in Ref 3. The governing equations (Ref 4) and constitutive model proposed to simulate the tensile test are presented in Sec. 3.

2. Experimental Setup and Procedure

Three alloys of titanium were evaluated during the experimental portion of this investigation. Nominal and measured alloy chemistries are shown in Table 1. Mill annealed sheet titanium of each alloy was fabricated into full thickness test specimens (Fig. 1), and exposed to simulated SPF conditions as shown in the third row of Table 2. Following the simulated SPF conditioning, the specimens were subjected to one of three post-processing methods, also described in Table 2. Tensile testing followed the method of ASTM E-8. After the completion of temperature conditioning and post processing, the different groups of specimens are measured and marked in the gage section to have a baseline for measuring % elongation.

Tensile testing was accomplished on a computer controlled SATEC test machine (Fig. 2a) with an attached extensometer (Fig. 2b). Specimens were loaded in the hydraulic grips, checked for alignment, fitted with the extensometer, and pulled to failure.

Load versus displacement data from the tensile test was collected by the digital data collection system attached to the SATEC test machine. The data were directly downloaded into a Microsoft Excel spreadsheet. Dimensions of the initial specimens and the failed section of the test specimens were entered into the spreadsheet. Plots of the load versus elongation for each specimen were recorded. Following the testing, the failed

Table 1 Titanium sheet material composition

Alloy chemistry	Weight % by inductively coupled plasma spectroscopy								
	Al	V	Mo	Sn	Zr	Cr	Si	Fe	O%[a]
Ti 6Al-4V (Ti 6-4)	6.25	4.23						0.2	0.160
Ti 6Al-2Mo-2Sn-2Zr-2Cr (Ti 6Q2)	5.93		2.05	2.12	2.14	1.04	0.23	0.03	0.107
Ti 5Al-3V-2Mo-2Fe (SP 700)	4.65	3.23	2.09					2.11	0.087

[a] Oxygen % determined using LECO TC-136 oxygen/nitrogen determinator

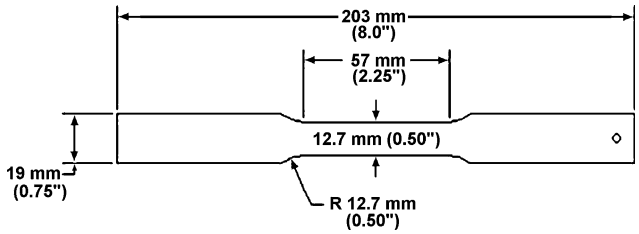

Fig. 1 Dogbone tensile specimens and dimensions

Table 2 Simulated SPF processing conditions and definition

Condition	Description
AR	As received, Mill annealed
AR + CM	AR with 0.127 mm (0.005") removed by chemical milling
AE	Simulated SPF conditioning. As exposed, 90 min in air furnace at either 788 °C, 845 °C or 885 °C followed by room air cool
AE + PP	AE with proposed, reduced processing—no chemical milling. Visible α case plus material representative of two cleaning cycles is removed by chemical cleaning. This simulates α case removal plus standard cleaning of an SPF part using existing processes.
AE + FP	AE with current production (full) processing, including chemical milling to remove 150% of the measured α case depth.

specimens were photographed and stored for possible further analysis.

3. Finite Element Modeling

Numerical simulations of the response of the tensile specimens were performed using the commercial Finite Element Analysis (FEA) code Ansys 8.0. The simulation consisted of modeling the reduced gage section of the specimens using two-dimensional four-node quadrilateral elements and representative finite element models for the front and side profiles as shown in Fig. 3a and b, respectively. Boundary conditions were prescribed in terms of specified displacements in order to maintain stability of the solution. The models were sufficiently constrained to suppress rigid body modes.

The non-linear constitutive relations from the experimental testing were fit using a Ramberg-Osgood relationship. The relationship consists of an additive decomposition of the elastic and plastic behavior of the material as

$$\varepsilon = \varepsilon_e + \varepsilon_p = \sigma/E + (\sigma/H)^{1/n} \quad \text{(Eq1)}$$

where ε is the material strain, subscripts e and p represent the elastic and plastic components, σ is the material stress, E is the elastic modulus, and H and n are specific Ramberg-Osgood parameters. The values for H and n were obtained by fitting

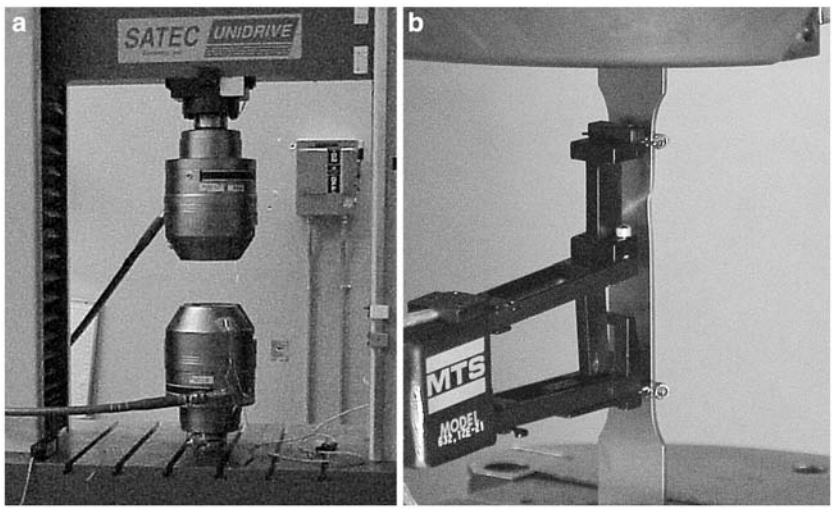

Fig. 2 Photograph of the experimental setup showing the (a) SATEC test frame and (b) close-up view of specimen installed with extensometer

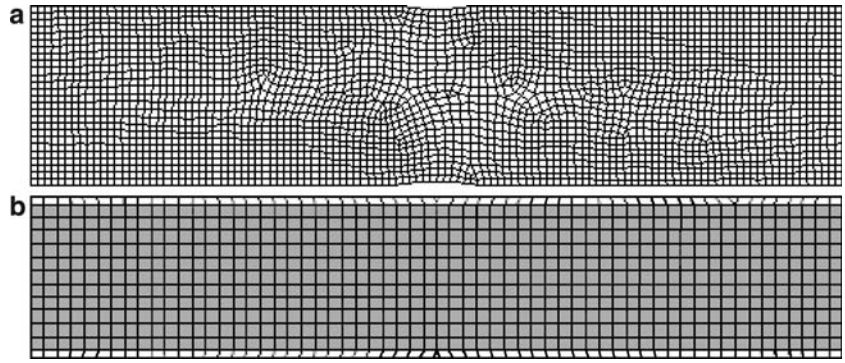

Fig. 3 Representative FEA mesh used for the gage section. (a) Front profile of the gage section including small perturbations in the form of small depressions on each side. (b) The side profile of the gage section including small perturbations in the form of small notches on the front and back sides

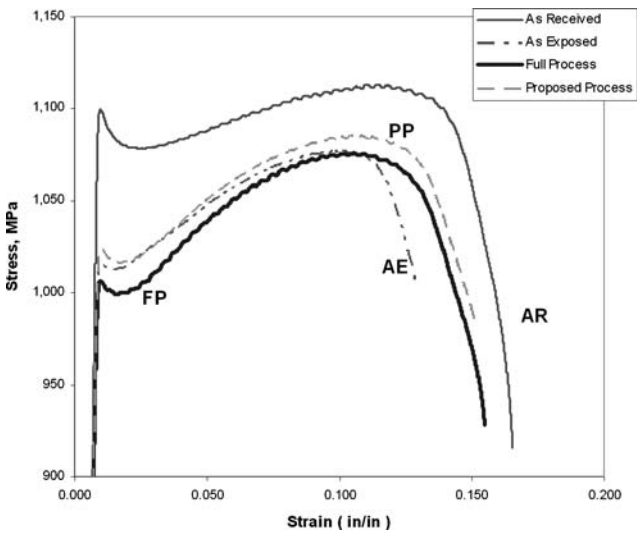

Fig. 4 Ti 6-4, 788 °C (1450°F) exposure tensile curves post-processing comparison

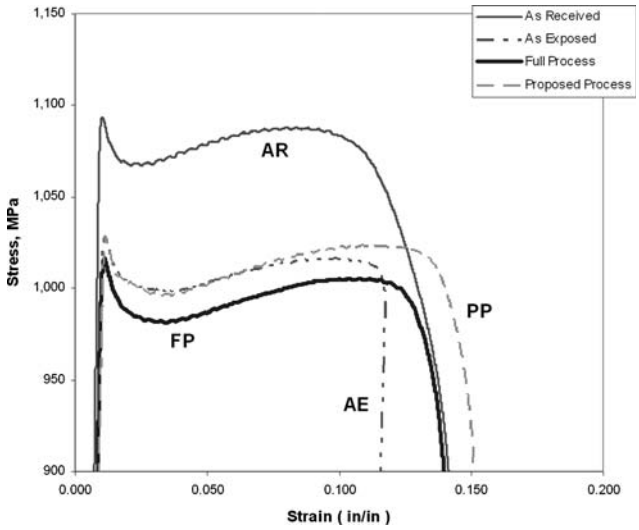

Fig. 5 SP 700, 788 °C (1450 °F) exposure tensile curves post-processing comparison

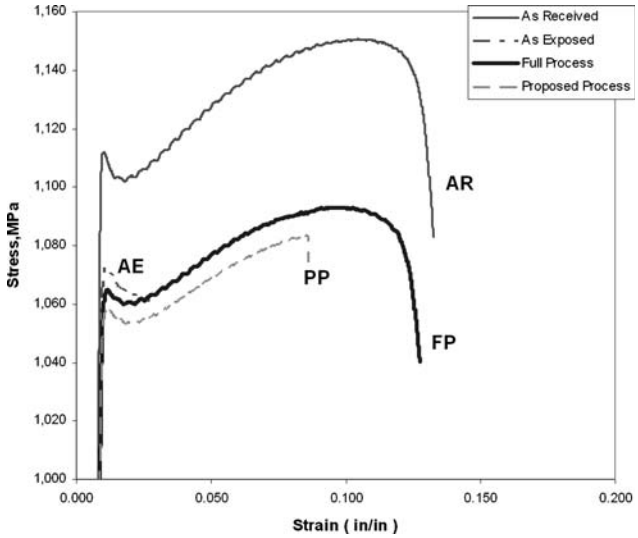

Fig. 6 Ti 6Q2, 788 °C (1450 °F) exposure tensile curves post-processing comparison

equation 1 to the experimental data using a least squares approach.

The behaviors for the different alloys were implemented within the finite element analysis code using a multilinear representation. Yielding was considered using J_2 plasticity, an associative flow rule and isotropic hardening. Large deformation and finite strain effects were also included. Plane stress models of the front profile (as shown in Fig. 3a) consisted of over 6000 degrees of freedom and plane strain models of the side profile consisted of over 2500 degrees of freedom (as shown in Fig. 3b). Small perturbations were included in the models (in the form of slight depressions or small notches) in order to ensure that failure, in the form of localized yielding, would occur in the center of the simulated gage length.

4. Experimental Tensile Stress-Strain Behavior

Figure 4-6 shows the stress versus strain graphs for the three alloys under different conditions. Figure 4 shows the stress versus strain curves for Ti 6-4 after the 788 °C (1450 °F)

Table 3 Table of results from experimental program

Material	Temp, F	Type	*E*, MPa	UTS, MPa	TYS, MPa	PA	*N*	*H*, MPa
Ti6Q2	1460	As received	126594.6	1160.691	1110.773	29	0.0439	1388.7
		As exposed	121120.3	1072.611	1072.57	7	0.055	1390.2
		Full process	116769.7	1093.164	1064.641	37	0.0467	1337.7
		Proposed process	116720.2	1083.567	1057.87	14	0.0424	1296.6
	1550	As received	110320.2	1012.764	1008.821	1	0.0462	1407.99
		Full process	111258.5	1116.806	1070.143	24	0.0311	1300.5
		Proposed process	114584	1124.018	1075.962	30	0.0298	1300.5
	1625	As exposed	100558	989.4739	975.6706	2	0.125	2187.8
		Full process	101657.1	1239.492	1092.985	20	0.0547	1603.3
		Proposed process	109122.4	1256.818	1150.915	30	0.057	1580.2
SP 700	1450	As received	120635	1093.233	1091.551	41	0.0211	1227.4
		As exposed	107314.9	1028.691	1028.595	25	0.0389	1215.9
		Full process	107389.7	1016.481	1015.757	46	0.0278	1162.5
		Proposed process	101738	1028.34	1027.671	33	0.0352	1213.67
	1550	As exposed	108734	1060.166	1030.884	7	0.0241	1313.1
		Full process	113003.4	1175.75	1124.915	34	0.0412	1462.2
		Proposed process	106620.2	1175.543	1091.992	40	0.0974	1678.8
	1625	As exposed	115524.3	1016.06	1016.06	3	0.0591	1603.2
		Full process	102530.1	1209.472	1146.199	20	0.0407	1487.98
		Proposed process	104594.6	1253.13	1202.694	21	0.0481	1626.7
Ti64	1450	As received	129130.7	1110.056	1096.267	−49	0.029	1280.9
		As exposed		NA	NA	NA	0.0492	1310.1
		Full process	129130.7	1075.879	1006.704	−50	0.0505	1306.5
		Proposed process	124470.4	1085.173	1022.948	−25	0.0371	1273.5
	1550	As exposed	125603.5	1078.175	1013.75	6	0.0365	1275.3
		Full process	127932.3	1148.653	1073.004	37	0.0375	1345.6
		Proposed process	118227	1108.126	1031.753	43	0.0446	1336.3
	1625	As exposed	120040.6	1044.136	1021.996	−5	0.0394	1297.5
		Full process	126319.2	1173.543	1088.186	33	0.046	1426.9
		Proposed process	110050.2	1148.805	1075.555	27	0.0401	1381.9

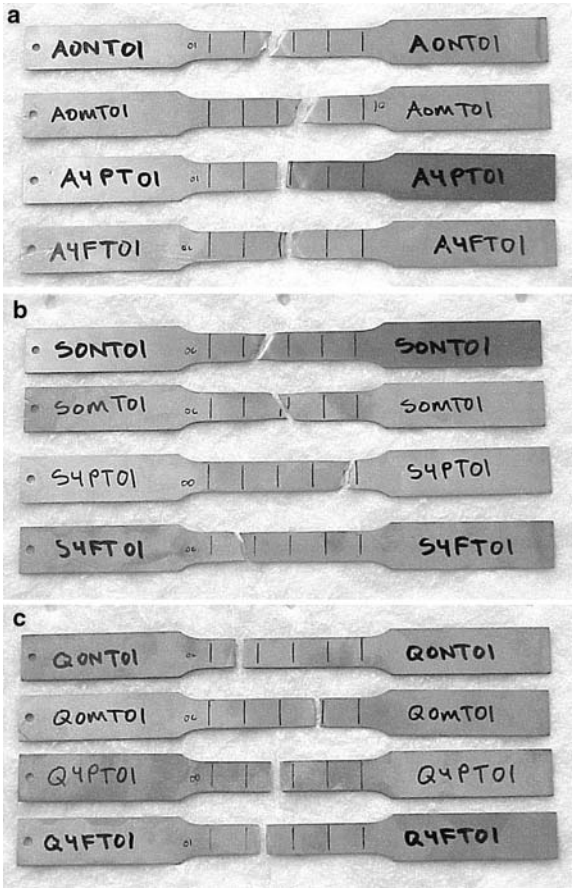

Fig. 7 Photographs of representative tensile specimens after testing: (a) Ti 6-4, (b) SP 700 and (c) Ti 6Q2

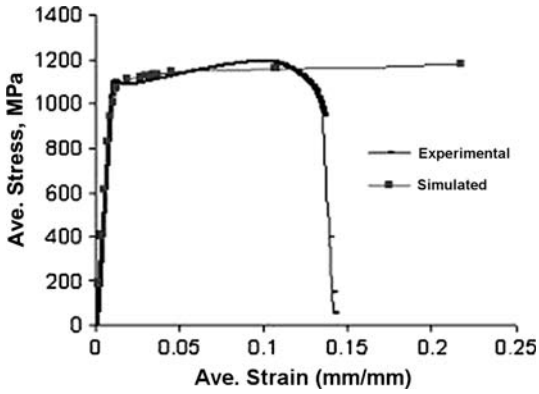

Fig. 8 Comparison of numerical and experimental stress-strain response for SP 700

conditioning cycle. Figure 5 shows the stress versus strain curves for the SP 700 material after the same lowest temperature conditioning cycle. The tensile behavior of the SP 700 is very similar to the Ti 6-4, with the AR condition showing the highest results and the AE condition the least amount of ductility. Prior to failure, the AE, PP, and FP curves are nearly the same, and similar to the Ti 6-4 curves.

The Ti 6Q2 tensile stress-strain curves are plotted in Fig. 6. The AR condition has higher strengths than any of the other conditions. While the AR and FP conditions are similar in overall behavior, the PP exhibits less ductility and the AE condition exhibits very little ductility. The Ti 6Q2 material shows the least amount of ductility of the three alloys in the AE condition and after PP post processing.

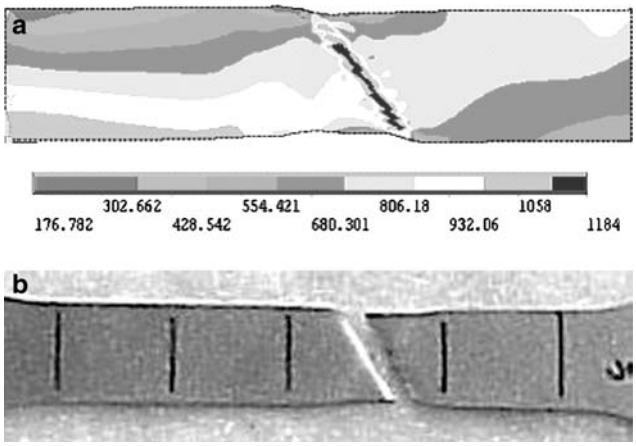

Fig. 9 (a) Contour plot of effective stress in the gage section of the SP 700 specimen in the as received condition at a relatively high applied average strain. (b) Representative photograph of fractured SP 700 as received specimen showing failure which occurred at approximately 45°

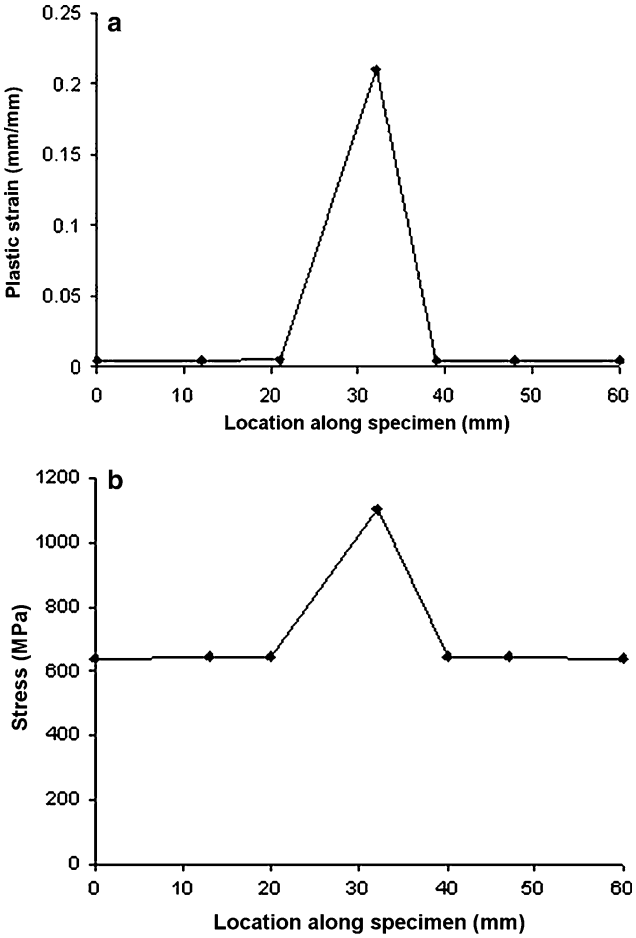

Fig. 10 (a) Plastic strain in the longitudinal direction and (b) stress in the longitudinal direction versus position along the gage length of the specimen

The results for the Ramberg-Osgood parameters that were obtained by fitting equation 1 to the experimental data using a least squares approach are shown in Table 3. Photographs of representative fractured specimens for the three different materials considered herein are shown in Fig. 7.

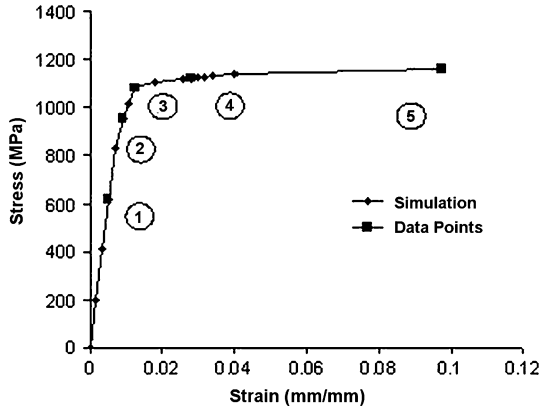

Fig. 11 Five points under consideration during the loading history of SP 700

5. Numerical Simulation Results

Figure 8 shows a plot of the stress-strain behavior for SP 700 from the numerical simulation, also shown are the experimental measurements. Here stress and strain are computed using the average stresses and strains extracted from element Gauss points along the gage length of the specimen. There is relatively good agreement between the two curves for low to moderate values of strain. Although some discrepancies in the average stress-strain curves appear at higher levels of deformation, it should be noted that such differences are approximately bounded within the experimental uncertainty range.

Figure 9(a) shows a contour plot of the effective stress in the gage section of the specimen of material SP 700 at temperature of 788 °C (1450 °F) at a relatively high applied strain after the onset of significant plastic deformation. Note that plasticity here results in the formation of a shear band through the gage section which occurs at an angle of approximately 45°. This band was consistent with experimental observations shown in Fig. 9(b). Figure 10(a) and (b) plot the plastic strain and the stress in the longitudinal direction as a function of position along the specimen showing the increase in magnitude in both the strains and the stresses near the shear band formation.

Let us explore more closely the evolution of the shear band formation in titanium alloy SP 700 by considering five separate instances during the simulation denoted by the squares in Fig. 11. These instances are identified as Point 1, Point 2, Point 3, Point 4, and Point 5 in the subsequent discussion.

Figure 12(a)-(d) shows plots of the effective stress, longitudinal component of stress, transverse component of stress and the shear stress, respectively, versus position along the specimen for the five designated points during the load history of SP 700. It is clear that at low level of applied elongation that the stresses are evenly distributed along the gage length of the specimen (Point 1). This is no longer the case as the applied elongation is increased to Point 2 where localization has already started to occur. Localization becomes more pronounced with further increase in the elongation.

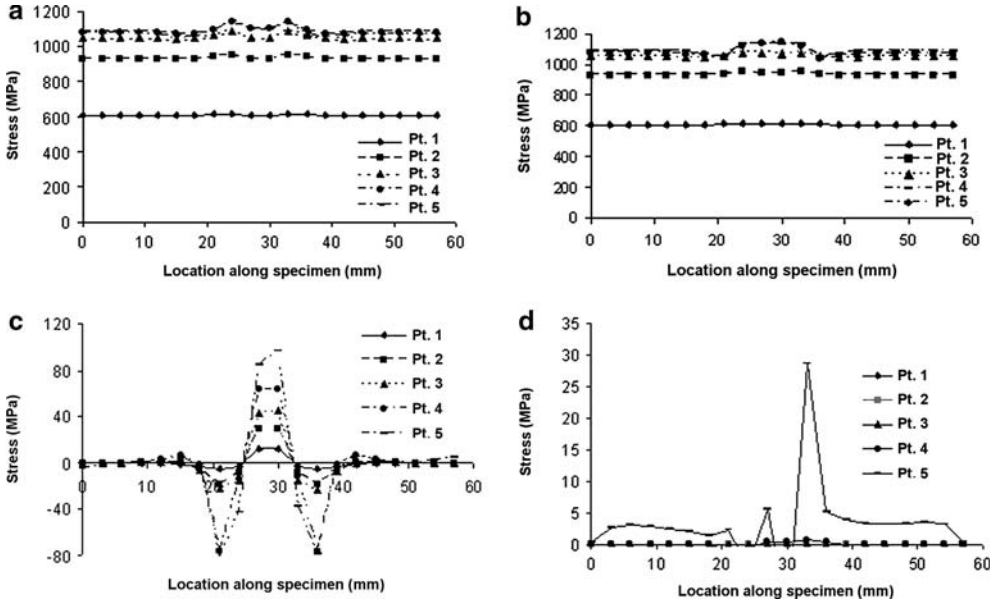

Fig. 12 Plots of (a) the effective stress, (b) longitudinal component of stress, (c) transverse component of stress and the (d) shear stress versus position along the specimen for the five points (pt1, pt2, pt3, pt4, pt5) during the load history of SP 700

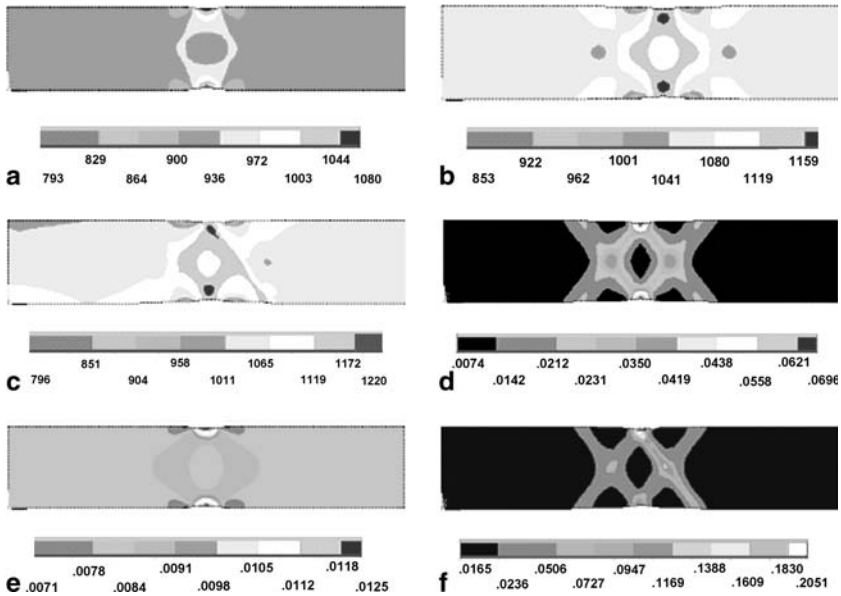

Fig. 13 Contour plots of the longitudinal component of stress in the specimen for average applied strain of (a) 0.009 mm/mm, (b) 0.283 mm/mm, and (c) 0.976 mm/mm and maximum principal strain in the specimen for average applied strain of (d) 0.009 mm/mm, (e) 0.283 mm/mm, and (f) 0.976 mm/mm

Figure 13 (a)-(c) shows contour plots of the evolution of the longitudinal component of stress in the specimen for average applied strain of (a) 0.009 mm/mm, (b) 0.283 mm/mm, and (c) 0.976 mm/mm, respectively. Figure 13 (d)-(f) shows contour plots of the maximum principal strain in the specimen for average applied strain of (d) 0.009 mm/mm, (e) 0.283 mm/mm, and (f) 0.976 mm/mm, respectively. It is clear that localization occurs quickly within the specimen due to the presence of the small perturbations. The localization is initially symmetrical with respect to both the longitudinal and vertical direction occurring at angles of plus and minus 45° from the perturbation; however, it becomes asymmetrical with additional applied elongation and ultimately leading to a single highly localized shear band.

The side profile including the brittle surface layer was modeled in order to explore the effect of process induced surface coating on the mechanical response. The brittle nature of the coating (α-case) was accounted for by assuming the presence of small notches in the outer layer of elements (see Fig. 3), which encompasses a more ductile inner core. These notches act as stress concentration points and ultimately increase the likelihood of yielding and hence premature failure of the specimen.

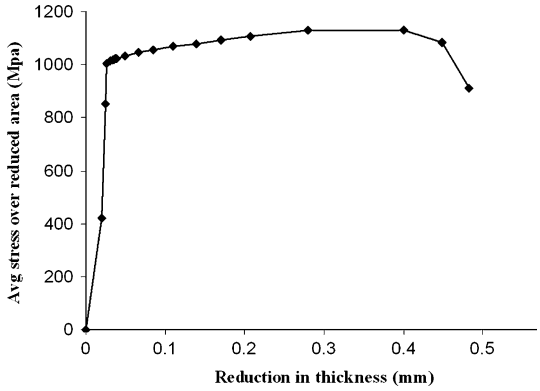

Fig. 14 Average stress over the reduced cross section versus reduction in cross sectional area for as exposed SP 700 processed at 788 °C (1450 °F)

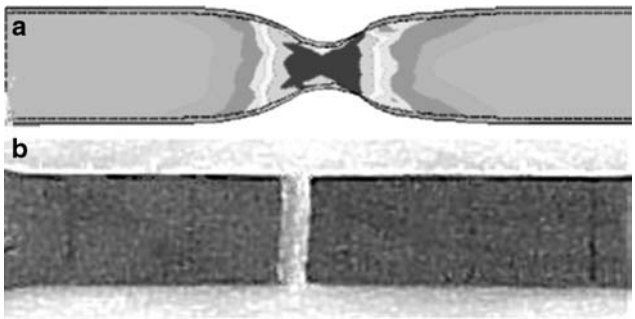

Fig. 15 (a) Contour plot of the effective stress over the side profile in a small portion of the gage section of the specimen. (b) Actual SP 700, as exposed to 788 °C (1450 °F) SPF conditioning showing failure 90° to the longitudinal direction

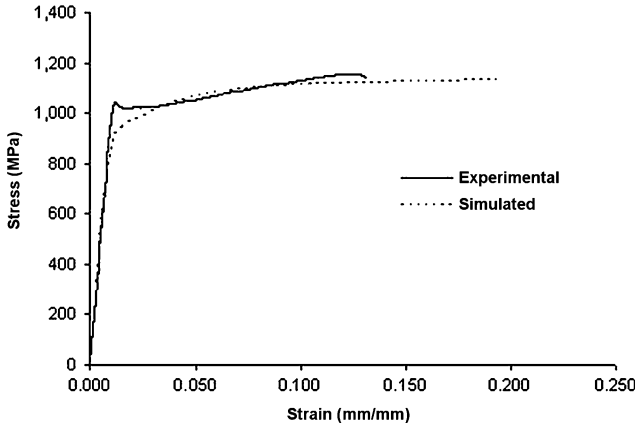

Fig. 16 Comparison of numerical and experimental response for SP 700 after 788 °C (1450 °F) conditioning and proposed method of post-processing (S4P)

Figure 14 plots the average stress over the reduced area versus the reduction in thickness for SP 700 in the as exposed, 788 °C (1450 °F) condition. Note that this specimen experienced a significant reduction in area at significantly low levels of applied elongation indicating a more brittle type behavior.

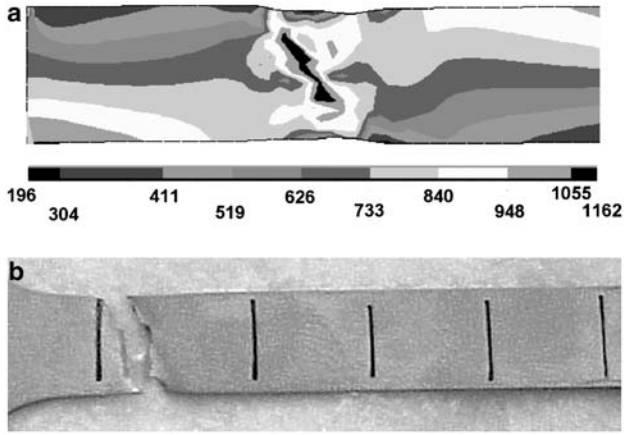

Fig. 17 (a) Contour plot of effective stress in the gage section of the specimen of material SP 700 in the S4P condition with a relatively high applied average strain

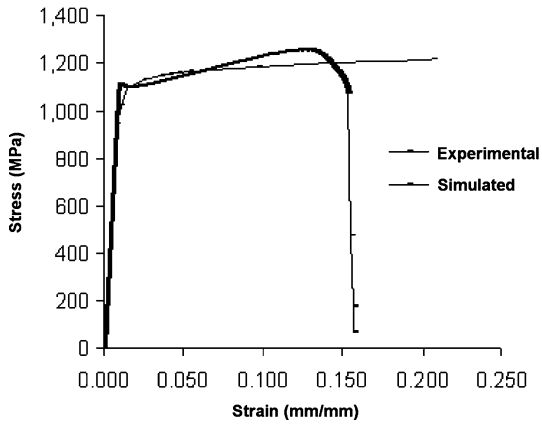

Fig. 18 Comparison of numerical and experimental response for Ti6-4 As received material

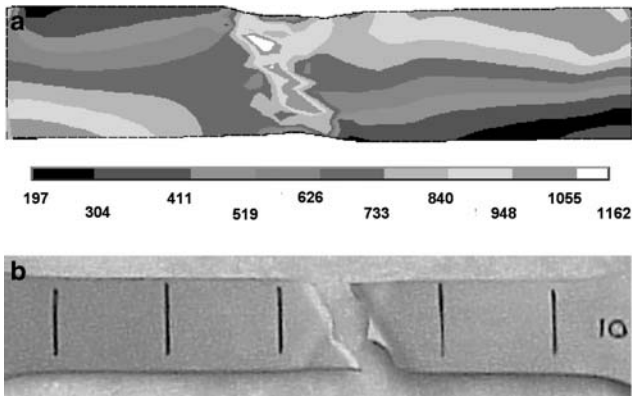

Fig. 19 (a) Contour plot of effective stress in the gage section of the specimen of material Ti6-4 as received at a relatively high applied average strain. (b) Corresponding photo of tensile tested specimen

Figure 15 shows the corresponding (SP 700, as exposed to 788 °C/1450 °F) contour plot for the effective stress over the side profile in a small portion of the gage section

of the specimen. It is clear that the maximum stress occurs at the necked region ultimately causing failure of the specimen. In this case, overall specimen failure would be expected to occur at 90° relative to the longitudinal axis of the specimen. This is consistent with experimental observations.

Figure 16 shows a comparison of the experimental and simulated stress-strain behavior for SP 700 after simulated 788 °C (1450 °F) SPF conditioning and subsequent proposed method of post processing (S4P). Figure 17 shows the corresponding contour plot of effective stress in the gage section at a relatively high applied average strain.

Figure 18 shows a comparison of the experimental and simulated stress-strain behavior for Ti6-4 as received material. The corresponding contour plot of effective stress in the gage section under a relatively high applied average strain is shown in Fig. 19.

6. Conclusions

Experimental and numerical analyses of mechanical behavior occurring in dogbone specimens during standard tensile testing have been presented. Characterization of the material response using dogbone specimens was performed first in order to obtain the experimental stress-strain relationship. Subsequently, an FEA model was used to simulate the tensile test. The necking and failure phenomenon have been described. Finally, a comparison of both the experimental and numerical simulation results have been verified. The proposed methodology has adequately described the mechanical, tensile test response of the SP 700 material in two different conditions and Ti 6-4 in the as received condition. Additional modeling of the response of Ti 6-4 after different conditions and the more brittle response of the Ti 6Q2 material is in work.

References

1. P. N. Comley, Manufacturing Advantages of Superplastically Formed Fine-Grain Ti-6Al-4V Alloy, *J. Mater. Eng. Perform.*, 2004, **13**(6), p 660–664
2. R. Gedney, Guide to Testing Metals Under Tension, *Adv. Mater. Process.*, 2002, **160**(2), p 29–31
3. F. Pitt and M. Ramulu, The Effect of Simulated SPF Exposure and Post Processing on the Tensile Properties of 3 Titanium Alloys, *First and Second International Symposia on Superplasticity and Superplastic Forming Technology, Proceedings from Materials Solutions 2001 and 2002*, D.G. Sanders and D.C. Dunand, Ed., ASM International, 2003, p 101–110
4. A. Higdon, E.H. Ohlsen, W.B. Stiles, J.A. Weese, W.F. Riley, *Mechanics of Materials*, 3rd ed., John Wiley & Sons, Inc., 1976